PAPER

Check for updates

Two new dammarane-type triterpenoids and other constituents from *Gymnosporia diversifolia* with anti-inflammatory and cytotoxic activities

Hanh Nhu Thi Hoang,†[a] Linh Thuy Thi Tran, [ID] †[b] The-Huan Tran, [ID] [b]
Nghia Ai Thi Doan,[b] Hung Quoc Vo,[b] Duyen Ngoc Thi Nguyen,[b] Hoai Thi Nguyen, [ID] [b]
Anh Tuan Le,[c] Hien Minh Nguyen [ID] [d] and Duc Viet Ho [ID] *[b]

Eighteen compounds were afforded from the aerial parts of *Gymnosporia diversifolia* collected in Vietnam. These included two new dammarane-type triterpenoids, gymnosporones A–B (**1–2**), fourteen previously identified triterpenoids (**3–16**), and two phenolic compounds (**17–18**). The structures of new components were elucidated by a combination of IR, HRESIMS, 1D-, 2D-NMR spectroscopic methods as well as by comparison with previously reported data. Compounds **3**, **7**, and **8** demonstrated inhibitory activity against NO production in RAW 264.7 macrophage cells, with IC_{50} values ranging from 71.85 to 95.71 μM. In cytotoxicity assays, compounds **1–3**, **7**, **8**, **11**, **15** and **16** exhibited moderate activity against A549, Hep-G2, and MCF-7 human cancer cell lines, with IC_{50} values between 10.65 and 47.78 μM. Among these, compound **15** was the most active, showing IC_{50} values of 10.65–14.28 μM across all tested cancer cell lines. *In silico* studies demonstrated that compounds **7** (-9.7 kcal mol^{-1}) and **11** (-9.4 kcal mol^{-1}) exhibited the strongest binding affinities for tubulin, whereas compound **15** showed strong dual binding to both tubulin (-8.7 kcal mol^{-1}) and BCL-2 (-9.1 kcal mol^{-1}). Molecular dynamics simulations confirmed the stability of ligand **15**–protein complexes and revealed a more favorable binding free energy for tubulin (-28.59 *vs.* -24.04 kcal mol^{-1}). Together with the *in vitro* results, these findings support a dual-target mechanism in which compound **15** may exert anticancer effects by inhibiting microtubule polymerization and inducing apoptosis. Our results highlight *G. diversifolia* as a rich source of structurally diverse triterpenoids with significant anticancer potential.

Introduction

The genus *Gymnosporia* (Wight & Arn.) Hook. f. (Celastraceae) comprises approximately 116 species worldwide. However, there are only twelve species have been phytochemical studied, with 80 compounds isolated.[1] Extracts and isolated compounds from this genus have shown valuable effects such as anticancer, anti-inflammatory, analgesic, antibacterial, antifungal, antiparasitic, antiviral, antioxidant, anti-ulcer, hepatoprotective, memory-enhancing, and inhibition of HIV-protease and PTP1B enzymes. Among these, the most prominent is the anticancer activity, with several potential compounds having been

discovered,[2–5] studied for their mechanism of action,[6–8] and tested in clinical trials.[9] Therefore, the *Gymnosporia* genus represents an important resource with significant potential for natural product-based drug discovery.

Gymnosporia diversifolia Maxim. [synonym: *Maytenus diversifolia* (Maxim.) Ding Hou, local name: "Lõa châu biển"] is a scrambling shrub, 3–4 meters tall, with small branches that form thorns.[10] Phytochemical investigation of this species remains limited. Several studies have described the presence of triterpenoids, flavonoids and alkaloids in the aerial parts of *G. diversifolia*.[11–13]

In our previous work, we identified several notable compounds from *Gymnosporia chevalieri* that exhibited anti-inflammatory and anti-proliferative activities.[1] As part of our ongoing investigation into the phytochemistry of the *Gymnosporia* genus, we have now isolated two new dammarane-type triterpenoids (**1** and **2**), along with sixteen known compounds (**3–18**), from the aerial parts of *G. diversifolia*. In this study, we report the isolation and structural elucidation of the new triterpenoids, as well as the evaluation of the nitric oxide (NO) production inhibitory activity and cytotoxicity of isolated compounds.

[a]*Faculty of Engineering and Food Technology, Hue University of Agriculture and Forestry, Hue University, 102 Phung Hung, Hue City, Vietnam*

[b]*Faculty of Pharmacy, Hue University of Medicine and Pharmacy, Hue University, 06 Ngo Quyen, Hue City, Vietnam. E-mail: hvietduc@hueuni.edu.vn*

[c]*Mientrung Institute for Scientific Research, Vietnam National Museum of Nature, Vietnam Academy of Science and Technology (VAST), 321 Huynh Thuc Khang, Hue City, Vietnam*

[d]*Research Group in Pharmaceutical and Biomedical Sciences, Faculty of Pharmacy, Ton Duc Thang University, 700000 Ho Chi Minh City, Vietnam*

† Authors with equal contribution.

Subsequently, molecular docking experiments were carried out to evaluate the binding affinities of the isolated compounds toward target proteins (tubulin and BCL-2), and the stabilities of the resulting ligand–protein complexes were further validated using molecular dynamics simulations.

Results and discussion

The chromatographic purification of the *n*-hexane and ethyl acetate fractions, partitioned from the methanolic extract from the aerial parts of *G. diversifolia*, afforded two new dammarane-type triterpenoids (**1** and **2**) and sixteen known compounds, including hydrodammarenone-I (**3**),[14] (20*R*,24*S*)-20,24-epoxydammar-3-one (**4**),[15] friedelin (**5**),[16] 4-epifriedelin (**6**),[17] canophyllol (**7**),[18] 3,4-secofriendelan-3-oic acid (**8**),[19] β-amyrin (**9**),[20] erythrodiol 3-acetate (**10**),[21] 3-acetyl-12-oleanen-28-oic acid (**11**),[22] 18α-oleanan-19α-ol-3-one (**12**),[23] uvaol (**13**), ursolic acid (**14**),[24] 30-hydroxy-20(29)-lupen-3-one (**15**),[25] lup-20(29)-ene-3β,30-diol (**16**),[26] methyl haematommate (**17**),[27] and α-tocopherol (**18**).[28] The chemical structures of the known components were verified by comparing their spectral data with those in the literature (Fig. 1).

Compound **1** was afforded as a white amorphous powder. The HRESIMS exhibited a sodiated molecular ion at *m/z* 481.36526 [M + Na]$^+$ (calcd for $C_{30}H_{50}O_3Na^+$, 481.36522),

corresponding to the molecular formula $C_{30}H_{50}O_3$, requiring six degrees of unsaturation. The appearance of hydroxy groups (ν_{max} 3455 cm^{-1}), double bond (ν_{max} 2968 cm^{-1}) and carbonyl group (ν_{max} 1684 cm^{-1}) in **1** was deduced by typical vibrations in IR spectrum.

The ^{1}H NMR spectrum of **1** exhibited the features of a terpenoid with almost signals appearing at δ_H less than 2.5 ppm. Several characteristic signals were observed including two olefinic protons [δ_H 5.71 (2H, overlapped, H-23 and H-24)], eight angular methyls [δ_H 1.33 (6H, s, H$_3$-26 and H$_3$-27), 1.12 (H$_3$-21), 1.08 (H$_3$-28), 1.04 (H$_3$-29), 1.01 (H$_3$-18), 0.95 (H$_3$-19), 0.88 (H$_3$-30) (each, 3H, s)] (Table 1).

The ^{13}C NMR spectrum of **1** displayed thirty signals. By using HSQC experiment, these were classified to eight CH$_3$ carbons (δ_C 30.0, 29.9, 26.7, 23.4, 21.0, 16.2, 16.0, 15.3), nine CH$_2$ carbons (δ_C 44.8, 39.9, 34.6, 34.1, 31.0, 27.4, 25.3, 22.0, 19.7), six CH carbons (δ_C 142.4, 122.0, 55.4, 50.0, 49.8, 42.5), and seven non-protonated carbons (δ_C 218.1, 75.4, 70.8, 50.0, 47.4, 40.3, 36.9). Furthermore, the signal at δ_C 142.4, 122.0, δ_H 5.71 (2H) was assigned to disubstituted double bond. The presence of one carbonyl carbon (δ_C 218.1), two oxygenated quaternary carbons (δ_C 75.4, 70.8) was also recognized in **1**. The above data suggested that compound **1** is a dammarane-type triterpenoid, which contains two hydroxy group, one ketone, and one double bond.
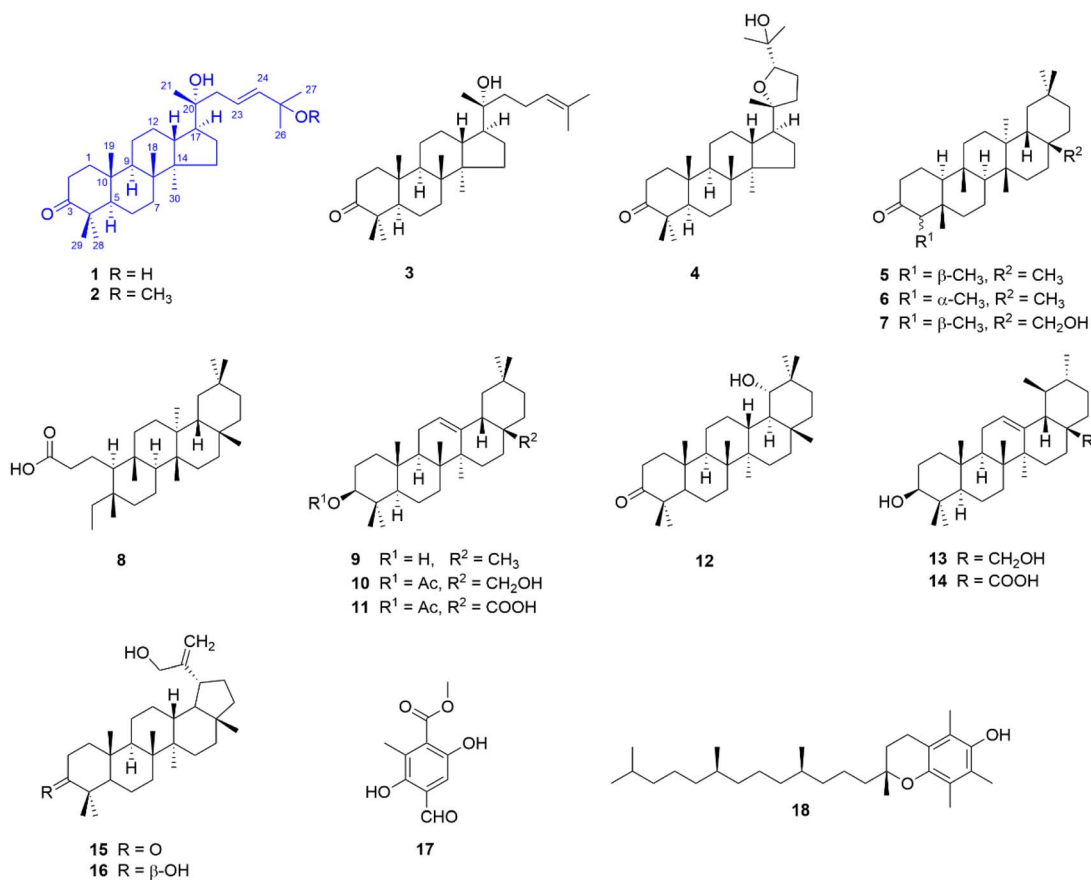

Fig. 1 Structures of compounds isolated from the aerial parts of *G. diversifolia*.

Table 1 ^{1}H and ^{13}C NMR data of **1** and **2** in CDCl$_3$ [δ (ppm), J (Hz)]

	1		**2**	
Position	$\delta_C{}^b$, type	$\delta_H{}^b$	$\delta_C{}^a$, type	$\delta_H{}^b$
1	39.9, CH$_2$	1.92^c	39.9, CH$_2$	1.93^c
		1.45 m		1.45 m
2	34.1, CH$_2$	2.49 m	34.1, CH$_2$	2.50 m
		2.43 m		2.44 m
3	218.1, C	—	218.1, C	—
4	47.4, C	—	47.4, C	—
5	55.4, CH	1.38 m	55.4, CH	1.37 m
6	19.7, CH$_2$	1.57^c	19.7, CH$_2$	1.57^c
		1.47 m		1.47 m
7	34.6, CH$_2$	1.57^c	34.6, CH$_2$	1.57^c
		1.31^c		1.31^c
8	40.3, C	—	40.4, C	—
9	50.0, CH	1.42 dd (12.3, 2.7)	50.0, CH	1.42 dd (12.3, 2.8)
10	36.9, C	—	36.9, C	—
11	22.0, CH$_2$	1.51 m	22.0, CH$_2$	1.50 m
		1.32^c		1.32^c
12	27.4, CH$_2$	1.94 m	27.5, CH$_2$	1.95 m
		1.25 m		1.26 m
13	42.5, CH	1.74^c	42.5, CH	1.74^c
14	50.0, C	—	50.0, C	—
15	31.0, CH$_2$	1.48 m	31.0, CH$_2$	1.48 m
		1.08^c		1.08^c
16	25.3, CH$_2$	1.74^c	25.3, CH$_2$	1.74^c
		1.32^c		1.33^c
17	49.8, CH	1.73^c	49.9, CH	1.73^c
18	15.3, CH$_3$	1.01 s	15.3, CH$_3$	1.01 s
19	16.0, CH$_3$	0.95 s	16.0, CH$_3$	0.95 s
20	75.4, C	—	75.4, C	—
21	23.4, CH$_3$	1.12 s	23.4, CH$_3$	1.13 s
22	44.8, CH$_2$	2.17 m	45.1, CH$_2$	2.20 m
23	122.0, CH	5.71^c	125.2, CH	5.66 dt (15.8, 7.4)
24	142.4, CH	5.71^c	139.5, CH	5.51 d (15.8)
25	70.8, C	—	74.9, C	—
26	30.0, CH$_3$	1.33 s	26.0, CH$_3$	1.27 s
27	29.9, CH$_3$	1.33 s	25.9, CH$_3$	1.27 s
28	26.7, CH$_3$	1.08 s	26.7, CH$_3$	1.08 s
29	21.0, CH$_3$	1.04 s	21.0, CH$_3$	1.04 s
30	16.2, CH$_3$	0.88 s	16.2, CH$_3$	0.87 s
OMe	—	—	50.3, CH$_3$	3.16 s

^{a} 150 MHz. ^{b} 600 MHz. ^{c} Overlapping signals.

As depicted in Fig. 2, the HMBC, COSY correlations allowed us to construct the planar structure of **1**. Particularly, the key HMBC correlations of H$_3$-28 (δ_H 1.08)/H$_3$-29 (δ_H 1.04) to C-3 (δ_C 218.1)/C-4 (δ_C 47.4)/C-5 (δ_C 55.4) implied that oxo group located

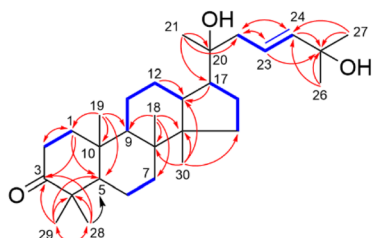**Fig. 2** Key HMBC (^{1}H → ^{13}C, arrows) and COSY (bold lines) correlations of **1**.

at C-3. In a similar manner, the HMBC cross-peaks from H$_3$-21 (δ_H 1.12) to C-17 (δ_C 49.8)/C-20 (δ_C 75.4)/C-22 (δ_C 44.8), from H$_3$-26, H$_3$-27 (δ_H 1.33) to C-25 (δ_C 70.8) positioned two OH groups at C-20, C-25, respectively. The double bond Δ^{23} was assigned by the COSY cross-peak of H$_2$-22 (δ_H 2.17) to H-23 (δ_H 5.71) as well as HMBC cross-peaks of H$_2$-22, H$_3$-26, and H$_3$-27 to C-24 (δ_C 142.4), of H-23 and H-24 to C-25. The *trans*-fused ring juncture of tetracyclic A/B/C/D system in dammarane skeleton was confirmed by NOESY experiment, as shown in Fig. 3. Therefore, compound **1** was proposed as 20,25-dihydroxydammar-23-ene-3-one.

The spectroscopic data of **1** was very similar to that of (20S,23E)-20,25-dihydroxydammar-23-ene-3-one (trivial name: isofouquierone).[29] However, a careful comparison of the ^{13}C NMR data of **1** with that of isofouquierone indicated that C-21 (δ_C 23.4) was upfield shifted, whereas C-20 (δ_C 75.4) and C-22 (δ_C 44.8) were downfield shifted [for isofouquierone: C-21 (δ_C 25.8), C-20 (δ_C 74.9), C-22 (δ_C 43.3)]. This finding suggested that the absolute configuration of C-20 chiral center is *R*. The 20*R* form of **1** was further strengthened by a good agreement of chemical shift of C-21 (δ_C 23.4) with those of 20*R*-hydroxydammarane derivatives [δ_C: 23.5 (dammarenediol-I, hydroxydammarenone-I (compound **3** in this study))], but significant different from those of 20*S* isomers [δ_C: 24.9 (dammarenediol-II), 24.7 (hydroxydammarenone-II)].[14] Consequently, structure of **1** was elucidated as (20*R*,23*E*)-20,25-dihydroxydammar-23-ene-3-one, and named gymnosporone A.

Compound **2** was isolated as a white amorphous powder. Its molecular formula ($C_{31}H_{52}O_3$) was established by HRESIMS data [sodiated molecular ion at *m/z* 495.38113 [M + Na]$^+$ (calcd for $C_{31}H_{52}O_3Na^+$, 495.38087)]. The NMR spectroscopic data of this isolate (Table 1) were very similar to those of **1**, except for signals showing the replacement of a hydroxy group (in **1**) by a methoxy group (in **2**). The presence of additional methoxy group was clearly deduced by a singlet signal at δ_H 3.16 (3H, s), which correlated to carbon at δ_C 50.3 in HSQC spectrum.

This group was further attached to the C-25 through the critical HMBC correlation from OMe (δ_H 3.16) to C-25 (δ_C 74.9). The occurrence of 25-OMe is accounted for the difference in δ_C values of the adjacent carbons (C-22 to C-27) between **1** and **2** (Table 1). Thus, compound **2** was elucidated to be (20*R*,23*E*)-20-hydroxy-25-methoxydammar-23-ene-3-one, and named gymnosporone B. It is important to mention that the analogue of **2** with 20*S* configuration was previously isolated from the floral spikes of *Betula platyphylla* var. *japonica*.[30] Again, the upfield shift of C-21 (δ_C 23.4) as well as downfield shifts of C-20
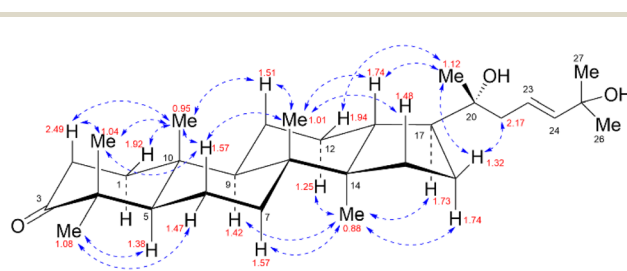

Fig. 3 Key NOESY correlations (dashed arrows) of **1**.

(δ_C 75.4) and C-22 (δ_C 45.1) of **2** comparing to those of 20*S* analogue [for (20*S*,23*E*)-20-hydroxy-25-methoxydammar-23-ene-3-one: C-21 (δ_C 26.0), C-20 (δ_C 74.9), C-22 (δ_C 43.7)] were observed.

Except for the well-known compounds (**9**, **13**, **14**, and **18**), the fourteen isolates were evaluated for their inhibitory effects on LPS-induced NO production in RAW 264.7 macrophage cells. Compounds **1**, **2**, **15**, and **16** exhibited significant cytotoxicity at 100 μM (cell viability ranging from 10.85 to 72.05%), which precluded their further evaluation in the NO inhibition assay. Based on the Griess assay results, only compounds **3**, **7**, and **8** demonstrated inhibitory activity against NO production, with IC$_{50}$ values ranging from 71.85 to 95.71 μM.

The cytotoxicity of isolates **1–8**, **10–12**, **15–17** was evaluated against A549 (lung), Hep-G2 (liver), and MCF-7 (breast) carcinoma cells, as well as HEK-293A (embryonic kidney) cells, using the SRB assay. Compound **15** emerged as the most active component, with IC$_{50}$ values ranging from 10.65 to 14.28 μM across the tested cancer cell lines. Compounds **1–3**, **7**, **8**, **11**, and **16** showed moderate activity, with IC$_{50}$ values in the range of 19.05–47.78 μM (Table 2). The remaining isolates were either inactive (compounds **4–6**, **12**) or only weakly active (compounds **10**, **17**).

Notably, triterpenoids **1–3** share structural similarities and exhibited significant cytotoxic effects, suggesting that the dammarane scaffold may be crucial for activity. Furthermore, while compound **5** was inactive, its hydroxylated derivative **7** displayed moderate activity (IC$_{50}$ = 22.37–39.32 μM), indicating that hydroxylation at C-28 may enhance cytotoxicity. Similarly, comparison between compounds **15** and **16** revealed that the presence of an oxo group at C-3 (in **15**) led to higher inhibitory potency than a hydroxy group at the same position (in **16**).

In this study, we found that 3,4-secofriedelan-3-oic acid (**8**) exhibited significant inhibitory activity against the tested cancer cell lines (IC$_{50}$ = 19.58–34.05 μM). Interestingly, a structurally related compound, 3,4-seco-29-hydroxyfriedelan-3-oic acid, which we isolated from *G. chevalieri*, also showed significant inhibition on these cell lines.[1] These observations suggested that the 3,4-secofriedelan-3-oic acid skeleton may play an important role in cytotoxicity.

Although the genus *Gymnosporia* is known for producing triterpenoids with diverse skeletons such as lupane, oleanane, ursane, and friedelane, the occurrence of dammarane-type triterpenoids is particularly rare.[1] The newly identified gymnosporones A and B (**1–2**) share the same dammarane backbone as hydroxydammarenone-I (**3**) but differ in their side-chain structures. Gymnosporone A (**1**) bears two hydroxyl groups at C-20 and C-25, whereas gymnosporone B (**2**) carries a methoxy substituent at C-25—an oxygenation pattern not previously observed among *Gymnosporia* triterpenoids. Both display the 20*R* configuration, in contrast to the common 20*S* isomers described in earlier studies.[29,30] These oxygenated substituents increase molecular polarity and may influence membrane permeability and protein interactions. Compounds **1–2** showed moderate cytotoxicity, suggesting that these modifications subtly modulate anti-proliferative activity compared with compound **3** and related analogues.

Structure–activity relationship analysis indicated that oxidation at C-3 is crucial for activity: compound **15** (3-oxo) was markedly more potent than its hydroxylated analogue **16**, highlighting the role of the carbonyl group. Hydroxylation at C-28 (compound **7** *vs.* **5**) also enhanced cytotoxicity, consistent with improved hydrogen bonding. The consistent potency of dammarane-type triterpenoids (**1–3**) emphasizes the importance of this hydrophobic tetracyclic scaffold.

The selectivity index (SI) was calculated as the ratio of IC$_{50}$ in HEK-293A normal cells to that in each cancer cell line to evaluate the safety and tumor selectivity of the isolated compounds.

Table 2 Inhibition of NO-production in LPS-stimulated RAW 264.7 cells and cytotoxicity against human cancer cells of isolated compounds

	IC$_{50}$[a] (μM) ± SD				
		Cytotoxicity			
Compound	Inhibition of NO-production	A549	Hep-G2	MCF-7	HEK-293A
1	NA	31.25 ± 1.21	23.82 ± 1.21	27.56 ± 1.15	24.75 ± 0.95
2	NA	31.09 ± 1.06	19.05 ± 0.47	22.15 ± 0.93	24.46 ± 0.67
3	95.71 ± 3.39	47.78 ± 3.85	25.63 ± 2.10	29.22 ± 1.34	34.08 ± 2.70
4	>100	>100	>100	>100	NT
5	>100	>100	>100	>100	NT
6	>100	>100	>100	>100	NT
7	79.94 ± 1.37	39.32 ± 1.29	22.37 ± 1.01	27.38 ± 1.19	30.08 ± 1.25
8	71.85 ± 2.41	34.05 ± 1.70	19.58 ± 1.93	27.01 ± 2.09	22.82 ± 1.09
10	>100	>100	72.84 ± 3.62	86.59 ± 4.66	97.19 ± 3.85
11	>100	42.37 ± 2.34	32.52 ± 2.28	37.59 ± 2.31	19.46 ± 1.55
12	>100	>100	>100	>100	NT
15	NA	14.28 ± 0.36	10.65 ± 0.40	12.19 ± 0.42	12.52 ± 0.37
16	NA	40.12 ± 0.87	29.98 ± 1.35	36.18 ± 1.18	43.22 ± 2.28
17	>100	>100	80.74 ± 3.59	99.3 ± 6.83	70.74 ± 4.44
Dexamethasone[b]	13.09 ± 1.13	—	—	—	—
Ellipticine[b]	—	1.71 ± 0.08	1.42 ± 0.08	1.54 ± 0.04	1.34 ± 0.08

[a] The half-maximal inhibitory concentration. [b] Positive control, NA: not available, NT: not tested.

A compound exhibiting an SI ≥ 2 is generally regarded as selectively cytotoxic toward cancer cells, whereas values close to or below unity indicate non-selective activity.[31,32] Most isolated compounds from *G. diversifolia* showed SI values of 0.8–1.2, suggesting similar sensitivity in normal and cancer cells. Compound 15, although the most potent, displayed SI values of 0.9–1.1, indicating only moderate selectivity.

Based on the cytotoxicity results, eight representative compounds (1–3, 7, 8, 11, 15, and 16) with noteworthy activity were selected for further *in silico* investigation. Two target proteins – tubulin (paclitaxel-binding site) and BCL-2 (BH3-binding groove) – were chosen to explore two major anti-cancer mechanisms: inhibition of microtubule polymerization and initiation of apoptosis.

As summarized in Table 3, docking revealed binding free energies of −7.4 to −9.7 kcal mol^{-1} for tubulin and −7.7 to −9.1 kcal mol^{-1} for BCL-2. Compounds 7 and 11 showed the strongest affinities for tubulin, whereas compound 15, which also exhibited the most potent *in vitro* cytotoxicity (IC$_{50}$ = 10.65–14.28 μM), achieved the highest affinity for BCL-2 (−9.1 kcal mol^{-1}) while maintaining a favorable interaction with tubulin (−8.7 kcal mol^{-1}). These data indicate that compound 15 can engage both targets with comparable binding strength, suggesting a potential dual-target mechanism.

Detailed interaction analysis of compound 15 highlighted distinct binding features in the two proteins (Fig. 4). Within the tubulin paclitaxel site, the ligand was stabilized predominantly by hydrophobic (van der Waals) contacts with core residues such as Leu286, Thr276, Phe272, Pro274, and Arg278. In contrast, binding to BCL-2 involved a more diverse interaction network, including a hydrogen bond with Asn143, an alkyl contacts with Met115, and multiple supporting van der Waals interactions. Taken together with the *in vitro* data, these docking results identify compound 15 as the most promising candidate for subsequent molecular dynamics (MD) simulations, aimed at validating the dynamic stability of its dual engagement with both tubulin and BCL-2.

A 100-ns MD simulation was performed for compound 15 in complex with tubulin and BCL-2, alongside the corresponding apo proteins. The presence of the ligand produced a marked
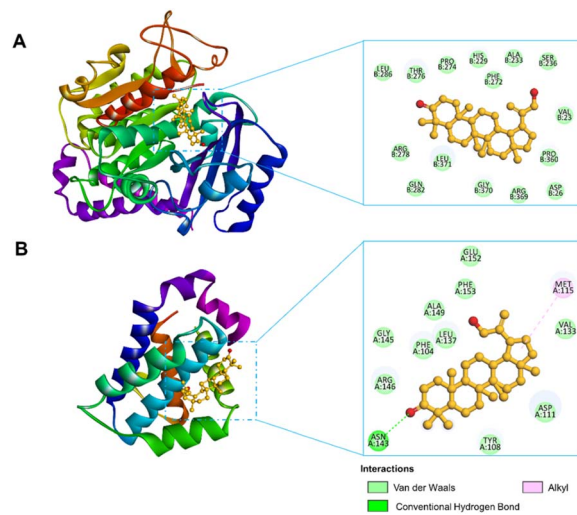

Fig. 4 Predicted binding interactions of compound 15 with (A) tubulin and (B) BCL-2, illustrated in 3D overview and 2D interaction diagrams.

stabilizing effect in both systems, albeit with distinct structural characteristics reflecting the nature of each binding pocket (Table S1).

For tubulin, the mean backbone root-mean-square deviation (RMSD) over the 100-ns trajectory decreased from 0.248 nm in the apo form to 0.219 nm in the complex, while the average Cα root-mean-square fluctuation (RMSF) decreased from 0.116 to 0.103 nm, indicating reduced global and local fluctuations upon ligand binding (Fig. 5 A and B). The average radius of gyration (R_g) and solvent-accessible surface area (SASA) values also declined slightly (2.177 → 2.157 nm; 196.0 → 192.4 nm^2), reflecting a more compact protein structure (Fig. 5C and D). Compound 15 remained stable, with an average ligand RMSD of only 0.056 nm throughout the 100 ns simulation (Fig. 5E). MM-

Table 3 Docking results of the compounds isolated from *G. diversifolia* on the two target proteins tubulin (PDB 1JFF) and BCL-2 (PDB 6O0K)

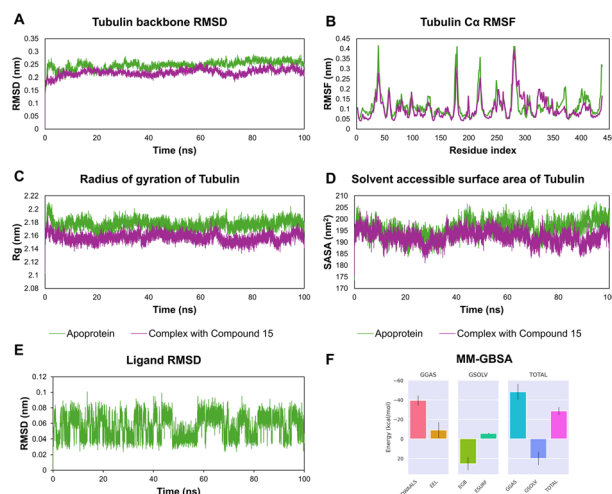| Compound	ΔG (kcal mol^{-1})	
	Tubulin	BCL-2
1	−8.6	−8.6
2	−8.3	−7.7
3	−8.2	−8.0
7	−9.7	−8.3
8	−8.1	−7.8
11	−9.4	−8.1
15	−8.7	−9.1
16	−8.3	−8.6
Ellipticine	−7.4	−8.3

Fig. 5 MD analysis (100 ns) of tubulin (PDB: 1JFF) in the apo state and in complex with compound 15: (A) backbone RMSD; (B) Cα RMSF; (C) radius of gyration (R_g); (D) solvent-accessible surface area (SASA); (E) ligand RMSD; (F) MM-GBSA binding free energy.

GBSA analysis yielded an average binding free energy ($\Delta G_{\text{binding}}$) of -28.59 ± 4.14 kcal mol^{-1}, dominated by favorable van der Waals (-39.53 kcal mol^{-1}) and electrostatic (-8.88 kcal mol^{-1}) interactions. This stabilization was partly offset by a strong unfavorable polar solvation term ($+25.31$ kcal mol^{-1}), while the non-polar solvation component (-5.50 kcal mol^{-1}) provided additional support (Fig. 5F and Table S2). Overall, the substantially negative binding energy underscores the high stability of the tubulin-**15** complex, where hydrophobic contacts within the paclitaxel site play a dominant role, complemented by moderate electrostatic contributions. These observations are fully consistent with the docking results.

For the BCL-2 complex, compound **15** produced a similar stabilizing effect. The mean backbone RMSD decreased from 0.142 nm (apo) to 0.135 nm (complex), and the mean Cα RMSF decreased from 0.081 to 0.072 nm (Fig. 6A and B).

In contrast to tubulin, however, the R_g and SASA increased slightly ($1.465 \rightarrow 1.470$ nm; $82.9 \rightarrow 83.7$ nm^2), indicating a modest local expansion of the BH3 groove to accommodate the steroidal framework of the ligand (Fig. 6C and D). In addition, compound **15** remained stable in complex with BCL-2, with an average ligand RMSD of only 0.045 ± 0.009 nm, indicating a sustained binding stability throughout the 100 ns simulation (Fig. 6E). MM-GBSA analysis yielded an average $\Delta G_{\text{binding}}$ of -24.04 ± 4.70 kcal mol^{-1}, driven primarily by favorable van der Waals (-31.93 kcal mol^{-1}) and non-polar solvation (-4.38 kcal mol^{-1}) contributions. Electrostatic interactions contributed modestly (-3.62 kcal mol^{-1}) and were largely counterbalanced by unfavorable polar solvation ($+15.90$ kcal mol^{-1}) (Fig. 6F and Table S2). These findings indicate that the stability of the BCL-**2**–**15** complex is governed mainly by hydrophobic interactions, consistent with the intrinsic hydrophobicity of the BH3-binding groove.

Collectively, these MD data demonstrate that compound **15** forms stable complexes with both tubulin and BCL-2, with

a more favorable binding free energy for tubulin (-28.59 vs. -24.04 kcal mol^{-1}). Together with the in vitro and docking results, these findings support a potential dual-target mechanism, in which compound **15** may exert antimitotic effects by stabilizing tubulin while simultaneously engaging the BH3 groove of BCL-2 to trigger apoptosis.

Experimental

General experimental procedures

Column chromatography was performed using silica gel (60 N, 40–50 μm, Kanto Chemical, Japan), YMC RP-18 (Fuji Silysia, Japan), and Sephadex LH-20 (Dowex® 50WX2-100, Sigma–Aldrich, USA). For analytical TLC, we used pre-coated silica gel 60F254 and RP-18 F254 plates (0.25 or 0.50 mm, Merck KGaA, Germany). All solvent ratios are given in volumes.

IR spectra were recorded using an IR Prestige-21 spectrometer (Shimadzu, Kyoto, Japan) with KBr pellets. Ultraviolet (UV) spectra were recorded in methanol using a Shimadzu UV-1800 spectrophotometer (Shimadzu, Kyoto, Japan). NMR data were acquired on a Bruker Avance Neo 600 spectrometer (Bruker, MA, USA) using TMS as the internal reference. HRESIMS data were obtained with a Xevo G2-XS QToF system (Waters, USA).

Plant materials

The aerial parts of G. diversifolia were collected from Quang Tri Province, Vietnam in November 2024. The plant material was identified by our co-author, Dr Anh Tuan Le, from the Mientrung Institute for Scientific Research, Vietnam National Museum of Nature, Vietnam Academy of Science and Technology. A voucher specimen (GD.01) has been placed in the Faculty of Pharmacy, Hue University of Medicine and Pharmacy, Vietnam.

Extraction and isolation. A total of 3.6 kg of dried aerial parts of G. diversifolia were ground into a fine powder and extracted three times at room temperature using 20.0 liters of methanol (MeOH) each time. The combined methanolic extracts were concentrated under reduced pressure, yielding 430 g of residue. This residue was then dissolved in water and successively partitioned with n-hexane and ethyl acetate (EtOAc) (2.0 L × 6 times for each solvent). The solvents present in the sub-extracts were then removed under vacuum to obtain the following fractions: n-hexane-soluble (H, 82.0 g), EtOAc-soluble (E, 75.2 g), and water-soluble (W, 201.8 g). The H fraction was further divided into five sub-fractions (H1–H5) through silica gel column chromatography, employing a gradient of n-hexane-acetone (100/0, 60/1, 40/1, 20/1, 10/1, 5/1, 2/1, 1/1, v/v), followed by 100% acetone.

Fraction H1 (38.2 g) was subjected to silica gel column chromatography using an n-hexane–acetone solvent gradient (50 : 1, 25 : 1, 20 : 1, v/v), resulting in six sub-fractions labeled H1A to H1F. Crude crystals formed in H1B were washed and recrystallized in acetone, yielding **5** (30.5 mg). Sub-fraction H1C (1.54 g) was further separated using a YMC RP-18 column with acetone–water (20 : 1, v/v) as the eluent, producing four sub-fractions (C1–C4). Compound **17** (15.3 mg) was isolated from
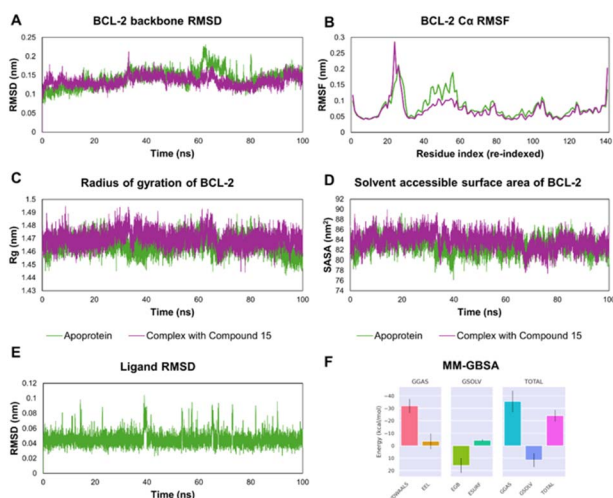

Fig. 6 MD analysis (100 ns) of BCL-2 (PDB: 6O0K) in the apo state and in complex with compound **15**: (A) backbone RMSD; (B) Cα RMSF; (C) radius of gyration (R_g); (D) solvent-accessible surface area (SASA); (E) ligand RMSD; (F) MM-GBSA binding free energy.

sub-fraction C1 (240 mg) *via* additional RP-18 chromatography using MeOH–water (2.5 : 1, v/v) as mobile phase. Sub-fraction C3 (350 mg) was purified first with Sephadex LH-20, eluting with MeOH 100%, followed by silica gel chromatography with *n*-hexane–dichloromethane (50 : 1, v/v) as an eluent, to yield **18** (211 mg). Sub-fraction C4 (200 mg) underwent silica gel chromatography, eluted by an *n*-hexane–dichloromethane system (50 : 1, v/v), producing three sub-fractions (C4.1–C4.3). Crystalline solids from C4.2 and C4.3 were recrystallized in acetone to afford **6** (15.8 mg).

Compound **9** (10 mg) was obtained from fraction H1E through RP-18 chromatography using acetone–water (10 : 1, v/v) as mobile phase. White needle-like crystals found in H1F were purified by RP-18 column chromatography, eluting with acetone–water (20 : 1, v/v), resulting in **12** (235 mg). The remaining portion of H1F (5.6 g) was fractionated on an RP-18 column, eluted by a gradient of acetone–water (3 : 1 and 5 : 1, v/v), producing six sub-fractions (F1–F6). Fraction F2 (800 mg) was separated using silica gel chromatography using *n*-hexane–acetone (10 : 1, v/v) as mobile phase, yielding sub-fractions F2.1–F2.4. From F2.4 (120 mg), compound **1** (5 mg) was isolated through sequential purification with RP-18 (acetone–water 3 : 1, v/v) and silica gel chromatography (dichloromethane–acetone 30 : 1, v/v).

Fraction F4 (1.6 g) underwent silica gel chromatography using *n*-hexane–acetone (20 : 1, v/v), generating seven sub-fractions (F4A–F4G). From F4C (250 mg), further separation using silica gel and an *n*-hexane–dichloromethane system (3 : 2, v/v) provided three fractions (C1–C3). Crystals from C3 were recrystallized in acetone to obtain **4** (17 mg). Similarly, white crystalline material from F4F was washed with MeOH to afford **7** (4.4 mg). Compound **11** (30 mg) was purified from F4G using RP-18 chromatography with acetone–water (5 : 1, v/v).

Fraction F5 (800 mg) was chromatographed on silica gel with *n*-hexane–dichloromethane (20 : 1, v/v), yielding seven sub-fractions (F5A–F5G). From F5B (1.0 g), compound **10** (7 mg) was isolated by RP-18 column chromatography using acetone–water (8 : 1, v/v) as mobile phase. Sub-fraction F5F (120 mg) was subjected to Sephadex LH-20 with dichloromethane–MeOH (1 : 1, v/v) as an eluent, followed by RP-18 chromatography with acetone–water (10 : 1, v/v) as mobile phase, to yield **3** (31 mg). Finally, crude crystals from fraction F6 were recrystallized in acetone to obtain **8** (30 mg).

The ethyl acetate (E) soluble fraction was applied to a silica gel column and eluted with a gradient of dichloromethane–MeOH (0 : 100 to 100 : 0), affording six fractions (E1–E6). Fraction E1 (5.83 g) was subjected to normal-phase column chromatography using dichloromethane–MeOH (60 : 1), yielding seven subfractions (E1A–E1G). Subfraction E1D (1.2 g) was separated on an RP-18 column with acetone–water (1 : 1), affording ten subfractions (E1D1–E1D10). Subfraction E1D6 (242.3 mg) was further purified by normal-phase chromatography using *n*-hexane–acetone (8 : 1), resulting in seven subfractions (E1D6A–E1D6G). Subfractions E1D6A (32.4 mg) and E1D6C (47.7 mg) were purified by Sephadex LH-20 chromatography with MeOH (100%), affording compounds **2** (20.0 mg) and **13** (27.2 mg), both as white powders. Subfraction E1D6E

(147.6 mg) was subjected to normal-phase chromatography with dichloromethane–acetone (30 : 1), then filtered and recrystallized from dichloromethane to give **14** (50.0 mg) as a white powder. Subfraction E1D8 (276.8 mg) was chromatographed on a silica gel column using *n*-hexane–acetone (9 : 1), affording **15** (17.3 mg) and **16** (23.8 mg), both as white powders.

Gymnosporone A (**1**): white amorphous powder; IR (KBr) ν_{max} (cm^{-1}): 3455, 2968, 1684, 1462, 1381, 1310, 1236, 1171, 1126, 1082, 980; UV (MeOH) λ_{max}: 219, 223 nm. ^{1}H NMR (CDCl$_3$, 600 MHz) and ^{13}C NMR (CDCl$_3$, 150 MHz): see Table S1; HRESIMS: m/z 481.36526 [M + Na]$^+$ (calcd for C$_{30}$H$_{50}$O$_3$Na$^+$, 481.36522).

Gymnosporone B (**2**): white amorphous powder; IR (KBr) ν_{max} (cm^{-1}): 3485, 2970, 2928, 2862, 1699, 1462, 1383, 1173, 1078, 986; UV (MeOH) λ_{max}: 218, 223 nm; ^{1}H NMR (CDCl$_3$, 600 MHz) and ^{13}C NMR (CDCl$_3$, 150 MHz): see Table S1; HRESIMS: m/z 495.38113 [M + Na]$^+$ (calcd for C$_{31}$H$_{52}$O$_3$Na$^+$, 495.38087).

Anti-inflammatory and cytotoxic assays. The cytotoxicity of the compounds was assessed using a sulforhodamine B assay on the A549, MCF-7, Hep-G2, and HEK-293A cells. To evaluate the *in vitro* anti-inflammatory effects, the NO production inhibitory activity in RAW 264.7 macrophage cells was measured. The concentration of nitrite in the culture medium, which serves as an indicator for the presence of NO, was determined using the Griess reaction. Detailed protocols for these experiments have been previously described in our reports for cytotoxic[33–35] and anti-inflammatory assays.[36]

Statistical analysis. The data are presented as the mean ± SD obtained from three independent experiments. The estimated half-maximal inhibitory concentration (IC$_{50}$) was calculated using TableCurve 2D software (v4.0, Systat Software Inc.).

Computational methods

Molecular docking. Ligand structures were drawn in Chem-Draw, converted to three-dimensional coordinates, and geometry-optimized using Open Babel.[37] The optimized ligands were then converted to PDBQT format with AutoDockTools.[38] Target proteins included tubulin (PDB ID: 1JFF)[39] and BCL-2 (PDB ID: 6O0K).[40] Protein structures were prepared by removing crystallographic water molecules, adding polar hydrogens, and assigning Kollman charges. Docking calculations were performed with AutoDock Vina,[41] using a grid box encompassing the entire co-crystallized ligand binding pocket. Binding free energies (ΔG, kcal mol^{-1}) and detailed ligand–protein interactions were analyzed with Discovery Studio Visualizer.

Molecular dynamics simulations. Protein–ligand complexes showing the most promising activities in both *in vitro* assays and docking, as well as the corresponding apo proteins, were subjected to MD simulations using GROMACS 2024.3 (ref. 42) with the CHARMM36 force field.[43] Ligand topologies and force-field parameters were generated by SwissParam.[44] Each complex was placed in a triclinic box, solvated with TIP3P water, and neutralized with Na$^+$/Cl$^-$ ions at a physiological concentration of 0.15 M. After energy minimization, the systems were equilibrated sequentially under *NVT* (1000 ps) and *NPT* (1000 ps) ensembles, followed by a 100 ns production run at 300 K and 1

atm. Trajectories were analyzed for RMSD, RMSF, R_g, and SASA. Binding free energies were estimated from the MD trajectories using the MM-GBSA method.[45] The system setup and analysis followed our previously established protocols with slight modifications.[46]

Conclusions

This is one of the rare phytochemical studies of *G. diversifolia*. From the aerial parts of this plant material, eighteen compounds have been isolated and structural identification. Gymnosporones A, B were identified as two new dammarane-type triterpenoids. Compounds **3**, **7**, and **8** exhibited NO inhibition in RAW 264.7 cells, with IC_{50} values in the range (71.85–95.71 μM). Compounds **1–3**, **7**, **8**, **11**, **15** and **16** exhibited moderate activity against A549, Hep-G2, and MCF-7 cancerous cells with IC_{50} values in the range (10.65–47.78 μM). *In silico* studies revealed that compound **15** binds strongly to both tubulin and BCL-2, supporting a dual-target mechanism through inhibition of microtubule polymerization and induction of apoptosis. MD simulations confirmed the stability of these interactions. Overall, *G. diversifolia* may contain bioactive triterpenoids of interest, among which compound **15** warrants further investigation as a possible anticancer agent.

Author contributions

Duc Viet Ho designed the study; Anh Tuan Le, Hanh Nhu Thi Hoang collected plant materials and performed extraction; Hanh Nhu Thi Hoang, Linh Thuy Thi Tran, Nghia Ai Thi Doan, Duc Viet Ho performed the isolation of compounds; Hung Quoc Vo, Duc Viet Ho clarified chemical structure of isolates; Hanh Nhu Thi Hoang, Nghia Ai Thi Doan, Duyen Ngoc Thi Nguyen, Hien Minh Nguyen, Hoai Thi Nguyen investigated *in vitro* biological activities; The-Huan Tran, Linh Thuy Thi Tran, Hien Minh Nguyen performed *in silico* study; Hanh Nhu Thi Hoang, Linh Thuy Thi Tran, Hoai Thi Nguyen, Duc Viet Ho analysed, drafted, and revised the manuscript. All authors read and approved the final manuscript.

Conflicts of interest

There are no conflicts to declare.

Data availability

Data supporting this study are included within the article and supplementary information (SI). Supplementary information: 1D- and 2D-NMR, IR, UV, and HRESIMS spectra of the new compounds, as well as molecular docking data for selected compounds. See DOI: **https://doi.org/10.1039/d5ra07080e**.

Acknowledgements

References

1 N. A. T. Doan, H. N. T. Hoang, A. T. Le, H. T. Nguyen, T. H. V. Le and D. V. Ho, *Nat. Prod. Res.*, 2025, **23**, 1–10, DOI: **10.1080/14786419.2025.2509886**.

2 (*a*) K. H. Lee, H. Nozaki, I. H. Hall, R. Kasai, T. Hirayama, H. Suzuki and R. Y. Wu, *J. Nat. Prod.*, 1982, **45**, 509–510; (*b*) Y. Kuo, C. H. Chen, L. M. Yang Kuo, M. L. King, T. S. Wu, S. T. Lu, I. S. Chen, D. R. McPhail, A. T. McPhail and K. H. Lee, *Heterocycles*, 1989, **29**, 1465–1468.

3 Y. H. Kuo, C. H. Chen, L. M. Kuo, M. L. King, T. S. Wu, M. Haruna and K. H. Lee, *J. Nat. Prod.*, 1990, **53**, 422–428.

4 Y. H. Kuo, M. L. King, C. F. Chen, H. Y. Chen, C. H. Chen, K. Chen and K. H. Lee, *J. Nat. Prod.*, 1994, **57**, 263–269.

5 Y. H. Kuo, J. C. Ou, K. H. Lee and C. F. Chen, *J. Nat. Prod.*, 1995, **58**, 1103–1108.

6 A. D. Alate, D. D. Khandalekar, A. J. Amonkar, M. K. Adwankar and M. B. Sahasrabudhe, *Biomedicine*, 1978, **28**, 270–273.

7 J. Z. Deng, D. J. Newman and S. M. Hecht, *J. Nat. Prod.*, 2000, **63**, 1269–1272.

8 D. Bhavita, B. Lakshmi and Z. Maitreyi, *Int. J. Pharm. Chin. Med.*, 2017, **1**, 000106.

9 F. Cabanillas, G. P. Bodey, M. A. Burgess and E. J. Freireich, *Cancer Treat. Rep.*, 1979, **63**, 507–509.

10 P. H. Ho, *An Illustrated Flora of Vietnam*, Tre Publishing House, Ho Chi Minh City, 2nd edn, 2000, pp. 151–153.

11 H. Zhi-sheng, Z. Yun-li, M. Guang-en, X. Ren-sheng and H. Qi-min, *J. Integr. Plant Biol.*, 1982, **24**, 360–365.

12 H. Nakao, K. Senokuchi, C. Umebayashi, K. Kanemaru, T. Masuda, Y. Oyama and S. Yonemori, *Biol. Pharm. Bull.*, 2004, **27**, 1236–1240.

13 N. Anoda, M. Matsunaga, M. Kubo, K. Harada and Y. Fukuyama, *Nat. Prod. Commun.*, 2016, **11**, 1085–1088.

14 J. Asakawa, R. Kasai, K. Yamasaki and O. Tanaka, *Tetrahedron*, 1977, **33**, 1935–1939.

15 Y. Hirose, T. Yanagawa and T. Nakatsuka, *Mokuzai Gakkaishi*, 1968, **14**, 59.

16 A. Mann, K. Ibrahim, A. O. Oyewale, J. O. Amupitan, M. O. Fatope and J. I. Okogun, *Am. J. Chem.*, 2011, **1**, 52–55.

17 X. J. Li, Z. Z. Liu, K. W. Kim, X. Wang, Z. Li, Y. C. Kim, C. S. Yook and X. Q. Liu, *Nat. Prod. Sci.*, 2016, **22**, 154–161.

18 Y. Z. Li, Z. L. Li, S. L. Yin, G. Shi, M. S. Liu, Y. K. Jing and H. M. Hua, *Fitoterapia*, 2010, **81**, 586–589.

19 S. A. Vieira Filho, L. P. Duarte, G. D. F. Silva, I. S. Lula and M. H. dos Santos, *Magn. Reson. Chem.*, 2001, **39**, 746–748.

20 Q. L. Ngo, P. T. Nguyen, V. M. E. Nguyen, T. N. T. Nguyen, N. T. Phan, K. K. M. Ngo, T. N. Ngo, N. M. Phan and T. P. Nguyen, *CTU. J. Innov. Sustain. Dev.*, 2023, **15**, 91–97.

21 M. R. Kim, H. H. Lee, K. S. Hahm, Y. H. Moon and E. R. Woo, *Arch. Pharm. Res.*, 2004, **27**, 283–286.

22 S. Nusan, N. H. Soekamto, F. Firdaus and Y. M. Syah, *J. Appl. Pharm. Sci.*, 2020, **10**, 135–141.

23 O. Wintersteiner, G. Krakower and M. Moore, *J. Org. Chem.*, 1965, **30**, 2847–2849.

24 V. N. Vu, T. H. Nguyen, T. H. Pham, T. H. Vu, N. T. Le, X. N. Nguyen, V. C. Pham and Q. V. Nguyen, *J. Anal. Sci.*, 2022, **28**, 1–6.

25 W. F. Tinto, L. C. Blair, A. Alli, W. F. Reynolds and S. McLean, *J. Nat. Prod.*, 1992, **55**, 395–398.

26 P. Van Kiem, C. Van Minh, H. T. Huong, N. H. Nam, J. J. Lee and Y. H. Kim, *Arch. Pharm. Res.*, 2004, **27**, 1109–1113.

27 B. Hickey, A. Lumsden, A. Cole and J. Walker, *N. Z. Nat. Sci.*, 1990, **17**, 49–53.

28 V. N. Odinokov, A. Y. Spivak, G. A. Emelyanova, M. I. Mallyabaeva, O. V. Nazarova and U. M. Dzhemilev, *Arkivoc*, 2003, **13**, 101–118.

29 P. G. Waterman and S. Ampofo, *Phytochemistry*, 1985, **24**, 2925–2928.

30 J. Xiong, M. Taniguchi, Y. Kashiwada, T. Yamagishi and Y. Takaishi, *J. Nat. Med.*, 2011, **65**, 217–223.

31 H. Atmaca, S. Ilhan, Ç. Ç. Pulat, B. A. Dundar and M. Zora, *ACS Omega*, 2024, **9**, 23713–23723.

32 R. Kaminsky, C. Schmid and R. Brun, *In Vitro Mol. Toxicol.*, 1996, **9**, 315–324.

33 V. D. Ho, T. Hoang, Q. H. Vo, V. K. Phan, T. A. Le, V. T. Pham, M. H. Nguyen, T. Kodama, T. Ito, H. Morita, A. Raal and T. H. Nguyen, *Phytochemistry*, 2017, **144**, 113–118.

34 H. T. Nguyen, L. T. T. Tran, D. V. Ho, D. V. Le, A. Raal and H. Morita, *Fitoterapia*, 2018, **130**, 100–104.

35 K. V. Nguyen, D. V. Ho, N. T. Le, K. Van Phan, J. Heinämäki, A. Raal and H. T. Nguyen, *Sci. Rep.*, 2020, **10**, 22193.

36 K. V. Nguyen, D. V. Ho, H. M. Nguyen, T. T. Do, K. V. Phan, H. Morita, J. Heinämäki, A. Raal and H. T. Nguyen, *J. Nat. Prod.*, 2020, **83**, 1201–1206.

37 N. M. O'Boyle, M. Banck, C. A. James, C. Morley, T. Vandermeersch and G. R. Hutchison, *J. Cheminf.*, 2011, **3**, 33, DOI: **10.1186/1758-2946-3-33**.

38 G. M. Morris, R. Huey, W. Lindstrom, M. F. Sanner, R. K. Belew, D. S. Goodsell and A. J. Olson, *J. Comput. Chem.*, 2009, **30**, 2785–2791.

39 J. Löwe, H. Li, K. H. Downing and E. Nogales, *J. Mol. Biol.*, 2001, **313**, 1045–1057.

40 R. W. Birkinshaw, J. N. Gong, C. S. Luo, L. Lio, E. White, A. K. Anderson, P. Czabotar and D. C. Huang, *Nat. Commun.*, 2019, **10**, 2385.

41 O. Trott and A. J. Olson, *J. Comput. Chem.*, 2010, **31**, 455–461.

42 M. J. Abraham, T. Murtola, R. Schulz, S. Páll, J. C. Smith, B. Hess and E. Lindahl, *SoftwareX*, 2015, **1–2**, 19–25.

43 A. Croitoru, S. J. Park, A. Kumar, P. Thangapandian, B. Patel, K. Patel, H. J. Lee, C. Lee and W. Im, *J. Chem. Theory Comput.*, 2021, **17**, 3554–3570.

44 M. Bugnon, M. Goullieux, U. F. Röhrig, J. Hert, D. Reker, S. Bianco, V. Zoete and O. Michielin, *J. Chem. Inf. Model.*, 2023, **63**, 6469–6475.

45 M. S. Valdés-Tresanco, M. E. Valdés-Tresanco, P. A. Valiente and E. Moreno, *J. Chem. Theory Comput.*, 2021, **17**, 6281–6291.

46 T. H. Tran, D. N. H. Doan, T. C. N. Cao, T. S. Tran and T. D. Tran, *RSC Adv.*, 2025, **15**, 16855–16868.